Multi-element dataset of soil profiles across climatic zones in China's mountains

Yuying Wu [a, b], Yuhan Wang [a, c], Wenzheng Yang [a], Jie Zhang [a], Yanhong Wu [a], Jun Li [d], Gan Zhang [d], Haijian Bing [a, *]

[a] Institute of Mountain Hazards and Environment, Chinese Academy of Sciences, Chengdu 610213, China

[b] University of Chinese Academy of Sciences, Beijing 10049, China

[c] Key Laboratory of Green Utilization of Critical Non-metallic Mineral Resources, Ministry of Education, Wuhan University of Technology, Wuhan 430070, China

[d] State Key Laboratory of Organic Geochemistry, Guangzhou Institute of Geochemistry, Chinese Academy of Sciences, Guangzhou 510640, China

[*] Corresponding author:

Haijian Bing (PhD), E-mail: hjbing@imde.ac.cn

Abstract

Datasets of soil multi-element concentrations are essential for advancing our understanding of ecological functioning and responses to global change in mountain regions. However, the paucity of such datasets represents a fundamental impediment to accurately assess and predict biogeochemical processes in these sensitive ecosystems. Here, we present a comprehensive geochemical dataset comprising more than 1,300 soil samples collected from 166 sites across 30 mountain regions in China, spanning five major climatic zones and representative vegetation types. Soil samples were systematically collected from three standardized horizons (organic, surface mineral, and parent material), and analyzed for the concentrations of 24 elements, including macronutrients (e.g., phosphorus, potassium, calcium, magnesium), micronutrients (e.g., iron, molybdenum, manganese, copper), and trace metals (e.g., cadmium, chromium, lead, antimony). To support integrated Earth system analyses, the dataset is accompanied by key site-specific environmental variables, including climate parameters (temperature, precipitation, aridity index), normalized difference vegetation index, soil physicochemical properties (pH, moisture, bulk density), soil type, parent rock type, atmospheric nitrogen deposition, and chemical index of alteration. The dataset reveals significant vertical stratification in element distributions, with organic horizon enriched in biogenic elements, and deeper horizons dominated by lithogenic components. Spatial patterns along latitudinal, longitudinal, and altitudinal gradients underscore the influence of climate and geology on soil chemistry. This open-access dataset provides a valuable resource for parameterizing and validating biogeochemical models, assessing soil quality in mountain regions, and improving predictions of ecosystem responses to global change. The dataset can be accessed via https://doi.org/10.11888/Terre.tpdc.302620 or https://cstr.cn/18406.11.Terre.tpdc.302620 (Wu et al., 2025b).

Key words: Mountain ecosystems, Soil dataset, Elementome, Soil profile, Multi-elements

1 Introduction

Mountain ecosystems, recognized globally as hotspots of biodiversity and critical regulators of Earth's biogeochemical cycles, are under increasing pressure from accelerating global changes (Antonelli et al., 2018; Wang et al., 2022) and anthropogenic impacts. The complex topography of mountain regions creates steep climatic and edaphic gradients over short spatial distances, generating distinct biogeochemical niches that are highly sensitive to environmental change (Dainese et al., 2024; Nogués-Bravo, 2007). Soils in these regions are central to ecosystem functioning, supporting primary productivity, nutrient cycling, and carbon sequestration (Cui et al., 2022; Sundqvist et al., 2013). However, our understanding of how these functions are regulated by the distribution and interaction of multiple soil elements remains limited, particularly under conditions of rapid global change (Kaspari and Powers, 2016; Tian et al., 2019; Wu et al., 2025a). A fundamental constraint hindering progress in this field is the scarcity of comprehensive, large-scale datasets that simultaneously quantify the distribution and interaction of a wide range of soil elements across diverse mountain landscapes. Overcoming this data deficiency is essential for unraveling the emergent properties of coupled biogeochemical cycles in these vulnerable ecosystems and for developing robust predictive models for their future integrity and resilience.

While the roles of key elements such as carbon (C) and phosphorus (P) in ecosystem processes are well established (Elser et al., 2010; Zuo et al., 2024; Wang et al., 2024), recent research highlights the importance of a broader suite of elements, including macronutrients, micronutrients, and trace metals, in shaping biogeochemical dynamics (Han et al., 2011; Vallicrosa et al., 2022). For instance, calcium (Ca), magnesium (Mg), and potassium (K) are essential for plant physiological processes (Fernández-Martínez et al., 2021; Peñuelas et al., 2019), while micronutrients such as molybdenum (Mo), copper (Cu), and manganese (Mn) function as critical cofactors in enzymatic pathways driving nitrogen fixation, methane oxidation, and organic matter decomposition (Dai et al., 2023; Hay et al., 2023). Furthermore, the intricate interplay between trace element availability and the structure and function of microbial communities is increasingly recognized as a key control on soil biogeochemistry (Giovannelli, 2023; Shafiee et al., 2021; Zhao et al., 2020). Conversely, elevated concentrations of toxic elements, including aluminum (Al), cadmium (Cd), chromium (Cr), and lead (Pb), can disrupt ecosystem integrity and impair ecosystem health through food chain transfer (Bing et al., 2016; Lynch and St. Clair, 2004; Nagajyoti et

al., 2010). Capturing the distribution and interactions of this wide range of elements is therefore indispensable for a mechanistic understanding of mountain ecosystem functioning (Fernández-Martínez et al., 2021; Kaspari and Powers, 2016; Vallicrosa, 2022).

Emerging evidence suggests that the composition and distribution of soil elements are regulated not only by individual environmental drivers such as climate, vegetation, and parent material, but also by complex interactions among these factors (Augusto et al., 2017; Haghverdi et al., 2019; Molina et al., 2024; Moreno-Jiménez et al., 2022). These interactions can lead to non-linear responses and threshold effects that are difficult to predict without comprehensive, spatially explicit datasets (Feng et al., 2024). Vertical stratification of elements along soil profiles further reflects the combined influence of biological inputs, weathering processes, and leaching losses, offering insights into long-term ecosystem development and nutrient cycling (Cronan et al., 2018; Kirkby, 2018; Jobbágy and Jackson, 2001; Steinnes and Lierhagen, 2018). For instance, biologically cycled elements tend to accumulate in organic-rich layers, while lithogenic elements are often more concentrated in deeper mineral layers or parent material (Jobbágy and Jackson, 2004; Agnan et al., 2019; Sayer et al., 2020). However, few studies have captured this vertical dimension across broad environmental gradients, and most existing datasets are limited in geographic scope, sampling depth, or the range of elements analyzed (Moreno-Jiménez et al., 2019; Ochoa-Hueso et al., 2023; Shangguan et al., 2014).

China's extensive and environmentally diverse mountain systems, which cover over two-thirds of the nation's terrestrial area, offer an exceptional natural laboratory for dissecting the complex interactions among climate, vegetation, geology, and soils that shape global biogeochemical cycles (Han et al., 2011). These mountains span a wide range of climatic zones, from tropical and subtropical rainforests to temperate forests, boreal forests, and alpine tundra, nearly including the full spectrum of Earth's terrestrial biomes (Kou et al., 2021; Lu et al., 2018). The combination of steep altitudinal gradients, varied parent materials, and diverse vegetation types results in a mosaic of soil environments that mirrors the global diversity of pedogenic conditions. Critically, many of these mountain regions remain relatively undisturbed by direct anthropogenic activities, providing a unique opportunity to assess natural controls on soil geochemistry and to establish baselines for detecting future environmental change. Here, we conducted a large-scale soil sampling campaign across 30 mountain ecosystems in China. These sites represent five major climatic zones and typical vegetation types in each region. A total of 1,314 soil

samples were collected from three standardized soil horizons (organic (O), surface mineral (A), and parent material (C)). Each sample was analyzed for the concentrations of 24 elements, including macronutrients, micronutrients, and trace metals. In addition, the dataset was integrated with a suite of ancillary variables, including satellite-derived vegetation indices, soil physicochemical properties, and climatic parameters. This dataset provides a rare, high-resolution view of multi-element distributions across spatial and vertical gradients in mountain soils. It enables cross-disciplinary analyses that link geochemical, ecological, and climatic processes, and serves as a critical resource for improving biogeochemical modeling, evaluating soil quality and ecosystem health, and understanding the resilience of mountain systems under global change.

2 Materials and methods

2.1 Study area

Soil samples were collected from 30 mountains located within accessible national and provincial nature reserves across China (Fig. 1). The study area spans a wide geographical range (18.9°N-53.5°N, 101.0°E-129.6°E, altitude: 210-4225 m above sea level). These sites represent diverse ecosystem zones, including tropical, subtropical, warm temperate, temperate, and cold temperate regions. Vegetation types include broadleaf forests, mixed broadleaf-coniferous forests, coniferous forests, and shrublands (Bing et al., 2021; Cui et al., 2022). The mean annual temperature (MAT) in the study area ranges between -5°C and 21°C, and the mean annual precipitation (MAP) varies between 223 mm and 1934 mm. Detailed information in each mountain can be found in Table 1.

2.2 Soil sampling

Sampling campaigns were conducted at 166 sites spanning 30 mountains between July 2012 and March 2013. In each mountain, sites were selected based on the altitude and dominant vegetation types. At each site, the geographic coordinate was recorded using a GPS device (eTrex Venture, USA). Three replicate plots (10 m × 10 m) were randomly established per site, spaced approximately 50 m apart to account for spatial heterogeneity. In each plot, soil profiles were manually excavated down to the parent material horizon. Soil horizons were delineated in the field based on morphological characteristics following the Chinese Soil Taxonomy (Chinese Soil Taxonomy Research Group, 2001; Yang et al., 2023). Horizon boundaries were determined through visual and tactile assessments (e.g., color, texture, consistency, moisture, and root distribution). Horizons were typically classified as O (organic), A (surface mineral),

and C (parent material) horizons. For each profile, the name, code, depth range, and diagnostic features were recorded. Soil samples were collected sequentially from bottom to up within each profile to avoid cross-pollution, with composite samples formed by homogenizing subsamples from each horizon. Samples were preserved in clean and sealed polyethylene bags and transported to the laboratory. A total of 1314 samples were obtained, comprising 381 from O horizon, 481 from A horizon, and 452 from C horizon. The limited pedogenic development in some mountain soils resulted in the absence of certain horizons in profiles. All samples were air-dried, and visible roots, litter, coarse fragments, and other debris were manually removed. The soils were then sieved through a 2 mm mesh prior to further analyses. At each sampling site, bulk density (BD) measurements were conducted adjacent to a representative soil profile. For mineral horizons, BD was determined using the standard cylindrical core method with stainless-steel rings. However, BD of the typically thin, organic-rich O horizon was measured by excavating pits of known volume. The volume of the excavated soils was quantified via water displacement by backfilling the pits (Maynard and Curran, 2007).

2.3 Soil physical and chemical analyses

Soil moisture content was determined by oven-drying the soils at 105℃ to constant mass, which was calculated using the following formula:

$$Moisture\ (\%) = \frac{Fresh\ weight - Dry\ weight}{Dry\ weight} \times 100\%$$

Soil pH was measured using a pH meter (Mettler-Toledo FE28, Switzerland) after shaking the soil samples with deionized water at a 1:2.5 soil-to-water ratio. Soil organic carbon (SOC) concentration was determined by a CE400 elemental analyzer (Elementar vario ISOTOPE cube, Germany), after removing carbonates with 5% HCl. Soil samples for element analysis were digested with concentrated HNO_3, HF, and $HClO_4$ (Bing et al., 2022). The concentrations of major elements (Al, Ba, Ca, Fe, K, Mg, Mn, Na, P, Sr, Ti, V, and Zn) in the digests were determined using an inductively coupled plasma atomic emission spectrometry (ICP-AES, Optima 2000, USA), and the concentrations of trace elements (Cd, Co, Cr, Cu, Mo, Ni, Pb, Sb, and Tl) were determined using an inductively coupled plasma mass spectrometry (ICP-MS, Agilent 7700x, USA), with SPEX^{TM} serving as the standard solution. Quality control was ensured by analyzing replicates, blanks, and reference material (GBW-07405, China). The recovery of the reference material was routinely within the range of 95-105%, and the precision and accuracy of the

analyses were < 5% (relative standard deviation).

2.4 Environmental data extraction and calculation

The MAT and MAP in the study area were collected from the WorldClim database (https://www.worldclim.org) with a resolution of 1 km. The aridity index (AI), calculated as the ratio of MAP to potential evapotranspiration (PET), was sourced from the Global Drought Index and Potential Evapotranspiration Database provided by the Plant Data Center of Chinese Academy of Sciences (doi.org/10.6084, CSTR:34735.11.PLANTDATA.0065, Zomer et al., 2022). The normalized difference vegetation index (NDVI) from 2001 to 2015 was derived from the Advanced Very High-Resolution Radiometer (AVHRR) dataset developed by the Global Inventory Modeling and Mapping Studies (GIMMS) group (https://ecocast.arc.nasa.gov/data/pub/gimms/3g.v1/), with a resolution of 1/12°. Atmospheric N deposition across China (1980-2015) were derived from Yu et al. (2019). Parent rock data for the SOTER geological reservoir at a scale of 1: 1000000 in Chinese provinces (1990) were obtained from the National Earth System Science Data Center (http://www.geodata.cn). The soil type data were digitized from the 1:1000000 Soil Map compiled by the National Soil Census Office in 1995 and obtained from the Resource and Environmental Science Data Center (https://www.resdc.cn).

The chemical index of alteration (CIA) was used to indicate the level of chemical weathering at each site (Nesbitt and Young, 1982).

$$CIA = \frac{Al_2O_3}{(Al_2O_3 + Na_2O + K_2O + CaO^*)} \times 100$$

where the oxide is given in molar ratio. The CaO* value represents the amount of CaO derived from silicate minerals and was corrected following the method proposed by McLennan (1993): when CaO ≤ Na_2O, CaO* is taken as the measured CaO content; when CaO > Na_2O, CaO* is assumed to equal Na_2O.

2.5 Data quality

The dataset was derived from extensive field sampling followed by laboratory analyses, and potential data errors may arise from both sampling and analytical procedures. During field sampling, strict adherence to standardized protocols was followed. Sample representativeness was ensured through replicate sampling, random collection within each site, and thorough homogenization of composite samples. Moreover, soil samples were analyzed in certified laboratories following standardized national protocols and rigorous quality assurance and quality control procedures. Analytical precision was

evaluated through repeated measurements, with relative standard deviations (RSD) of major elements determined by ICP-AES being below 3%, and RSD of trace elements determined by ICP-MS being below 5%. Accuracy was assessed using the certified reference material (GBW-07405, China), with recoveries ranging from 95% to 105%. Before the analysis of soil data, outlier detection was performed to ensure dataset reliability.

2.6 Statistical analysis

All statistical analyses were conducted using R (version 4.3.1). To test differences in element concentrations among soil horizons, we employed linear mixed-effect models using the "lmer" function from the "lme4" package, where soil horizon was treated as a fixed factor and sampling site as a random factor. Regression analyses were conducted to examine the spatial distribution characteristics of each element. To explore the compositional differences in elemental assemblages across soil horizons and to assess the influence of environmental variables on soil element variation, redundancy analysis (RDA) was conducted using the "rda" function in the "vegan" package. Correlation analyses were conducted separately for each soil horizon to identify horizon-specific relationships between elemental concentrations and environmental drivers. Furthermore, we employed the "randomForest" and "rfPermute" packages to perform random forest analyses for each soil horizon, aiming to evaluate the explanatory power of environmental factors on elemental variation and to assess their relative importance.

3 Data description and evaluation

This dataset provides a comprehensive and continental-scale characterization of soil element composition across China's mountains, spanning five major climatic zones and three pedogenetically distinct soil horizons. The dataset includes quantitative measurements of 24 elements, thereby offering a holistic view of soil geochemistry in mountain regions. The dataset integrates information from extensive field surveys, laboratory analyses, high-resolution satellite-derived vegetation indices, and ancillary environmental data compiled from national and global databases. To ensure data consistency and comparability across sites, all soil samples were collected following standardized sampling protocols and analyzed using uniform laboratory procedures and instrumentation. In total, nine key environmental drivers were compiled and categorized into four groups, including climate variables (e.g., MAT, MAP, AI), vegetation characteristics (e.g., vegetation type, NDVI), basic soil properties (e.g., pH, moisture), and atmospheric nitrogen deposition levels. These integrated variables enable robust evaluation of the interactions

between environmental factors and element distributions in soils.

3.1 Elemental concentrations across soil horizons

Elemental concentrations in mountain soils exhibited a wide dynamic range, spanning over six orders of magnitude. The highest mean concentration was observed for SOC (127,699 mg/kg), while the lowest was for Tl (0.56 mg/kg, Fig. 2). The overall elemental mass ratio follows the pattern of C_{227038} : Al_{100998} : Fe_{46599} : K_{30204} : Ca_{19164} : Na_{14734} : Mg_{12201} : Ti_{5809} : P_{1373} : Mn_{1271} : Ba_{839} : Sr_{233} : Zn_{171} : V_{102} : $Cr_{87.1}$: $Pb_{71.1}$: $Ni_{30.3}$: $Cu_{28.4}$: $Co_{13.2}$: $Be_{3.31}$: $Sb_{2.92}$: $Mo_{2.04}$: $Cd_{1.18}$: Tl_1, underscoring the compositional diversity shaped by both natural and anthropogenic processes in mountainous environments.

Pronounced stratification of elemental concentrations was observed across the three soil horizons (Fig. 3). The O horizon, enriched in organic matter, exhibited significantly higher concentrations of major elements (e.g., carbon, Ca, and P), alongside elevated levels of several trace elements (e.g., Cd, Mn, Zn, Pb, and Sb). This enrichment pattern is consistent with the accumulation of both biogenic nutrients and atmospherically deposited pollutants. In particular, the elevated concentrations of Cd, Pb, and Sb in the O horizon reflect anthropogenic inputs through long-range atmospheric transport and subsequent deposition (Bing et al., 2019, 2021). These findings reinforce the role of the O horizon as a critical biogeochemical interface where atmospheric inputs are retained and processed. In contrast, lithogenic elements such as Al, Fe, K, Na, Mg, Ti, Sr, and V showed increasing concentrations with depth, particularly in the A and C horizons (Fig. 3). This trend reflects the growing influence of parent material composition and geochemical weathering processes with depth, where the contributions from organic matter decline and pedogenic processes such as mineral dissolution and secondary mineral formation dominate (Agnan et al., 2019; Kirkby et al., 2018; Woodruff et al., 2009). The systematic increase in these elements suggests long-term pedogenic accumulation, consistent with the downward translocation of weathering minerals and reduced biological cycling in subsurface horizons. Overall, this vertical differentiation of elemental concentrations across soil horizons underscores the combined effects of biological activity, atmospheric deposition, and geochemical weathering in shaping the composition and distribution of soil elements in mountainous ecosystems.

3.2 Spatial distribution of soil elements across China's mountains

The spatial distribution of soil elements across China's mountains reveals complex patterns along latitudinal, longitudinal, and altitudinal gradients (Fig. 4), indicating the integrated influence of climatic,

239 geological, and biological factors. Latitudinal trends in element concentrations were evident for several
240 elements. Notably, concentrations of K, Mn, Mo, Ba, and Sr increased consistently with latitude,
241 reflecting latitudinal variation in temperature-mediated weathering processes and element cycling
242 (Moreno-Jiménez et al., 2022). In contrast, elements such as Ca, Mg, Na, Ni, Cu, Cd, Co, and Zn
243 exhibited unimodal distribution patterns, with peak concentrations in mid-latitude regions, particularly
244 at Mts. Suyukou, Wuyuezai, and Guandi. These non-linear patterns may arise from the combined
245 influence of regional precipitation regimes, variable soil development stages, and differential
246 atmospheric deposition (Bing et al., 2021; Luo et al., 2016a; Ren et al., 2019). Site-specific anomalies
247 were also observed, indicating the strong influence of localized geological conditions. For instance, the
248 high Ca concentrations at Mt. Gongga and elevated Ba and Sr concentrations at Mt. Dabie are attributed
249 to distinctive lithological features and mineralogical compositions at these locations, which can override
250 broader climatic or biogeographical trends (Yang et al., 2015; Zhi et al., 2004).

251 Elemental distributions along the longitudinal gradient also exhibited significant patterns.
252 Concentrations of Mn, Mo, and Zn increased from west to east across the study area, while Mg, Cr, and
253 V showed declining trends in the same direction (Fig. 4). Phosphorus exhibited a non-monotonic
254 longitudinal pattern, with concentrations decreasing initially and then increasing towards the eastern
255 regions. These longitudinal patterns may reflect transitions in geologic substrates, soil parent materials,
256 and regional differences in anthropogenic influence (Yang et al., 2022). Altitudinal variation in soil
257 elemental concentrations further highlights the influence of mountain-specific environmental gradients.
258 Concentrations of certain heavy metals (e.g., Cd, Cr, and V) increased significantly with altitude, while
259 Cu and Ni exhibited unimodal distribution patterns (Fig. 4). These altitudinal patterns are likely shaped
260 by altitude-driven shifts in local climatic conditions, vegetation type, and soil-forming processes, as well
261 as differences in parent material exposure and erosion dynamics (Moreno-Jiménez et al., 2022; Yang et
262 al., 2022).

263 **3.3 Environmental drivers of soil element composition**

264 The elemental composition of soils across China's mountains is significantly influenced by a combination
265 of climatic, edaphic, and biogeographic factors. Statistical analyses revealed that variables such as MAT,
266 MAP, AI, NDVI, CIA, soil pH, latitude, and soil moisture were significantly correlated with the
267 concentrations of multiple elements ($p < 0.05$, Fig. 5). Climate- and vegetation-related variables showed

negative correlations with SOC, P, Ca, Mg, Na, Mn, Ba, and Sr ($p < 0.05$). These relationships suggest that cooler and drier sites, typically at higher altitudes or in arid regions, tend to accumulate higher concentrations of these elements, due to reduced microbial decomposition, slower organic matter turnover, and limited leaching under low-temperature and low-precipitation conditions (Moreno-Jiménez et al., 2019, 2023). Conversely, warmer and more vegetated environments may enhance biological cycling and leaching, leading to lower elemental retention in soils. Soil pH emerged as a key factor influencing elemental availability and retention. Most elements (except SOC, Fe, Sb, Pb, Tl, and Ti) exhibited positive correlations with pH (Fig. 5), indicating that higher pH conditions favor the retention or reduce mobility of these elements. This pattern reflects the well-established role of pH in controlling solubility, adsorption, and precipitation processes in the soil matrix (Barrow et al., 2023). Distinct vertical patterns in elemental composition were observed across soil horizons, reflecting the transition from biologically active surface layers to more geochemically stable subsurface zones (Bing et al., 2021; Cronan et al., 2018; Jobbágy and Jackson, 2001). The O horizon exhibited elevated concentrations of SOC, P, Ca, Sr, and Cd, corresponding to inputs from plant litter, root exudates, and atmospheric deposition. The A horizon showed intermediate concentrations, indicating a mixing zone influenced by both surface biological activity and subsurface geochemical processes. The C horizon was enriched in lithogenic elements such as Ti, Al, Fe, and V, consistent with its proximity to parent material and dominance of mineral weathering processes.

The explanatory power of environmental drivers varied by both elements and horizons (Fig. 6). In the O horizon, the model demonstrated generally high explanatory power ($R^2 > 60\%$) for most elements. For example, soil pH contributed strongly to the variability of Ca, while the variation in P was primarily driven by pH, precipitation, and vegetation indices. These results highlight the strong influence of biological processes, climate, and atmospheric deposition on the biogeochemical cycling and accumulation of elements in the organic-rich soils. In the A horizon, the explanatory power remained high, and the explained variance of some elements such as P, K, Ca, Mg, and Al slightly increased compared with the O horizon. The relative importance of CIA, moisture, and pH became more pronounced across a broader set of elements, suggesting the critical role of weathering and pedogenic processes in this horizon. In the C horizon, explanatory power was variable, with relatively low R^2 values for SOC (< 30%), Cd, and Mn, but remaining high for other elements. Na exhibited particularly high

297 explained variance, consistent with its close association with the weathering of Na-rich parent minerals.
298 A prominent trend in the C horizon was the widespread and strong influence of pH and CIA on a majority
299 of elements, often exceeding their importance in the O and A horizons. This underscores the dominant
300 role of deep geochemical stabilization, mineral transformation, and parent material composition in
301 controlling element distributions at greater depths. Overall, the influence of environmental factors on
302 SOC and other biologically cycled elements decreased markedly with depth, consistent with the reduced
303 biological activity and increasing geogenic control in subsurface horizons (Jobbágy and Jackson, 2001;
304 Sayer et al., 2020). In contrast, pH and CIA became progressively more influential in the A and C horizons,
305 highlighting the increasing importance of geochemical and mineral processes.

306 **4 Potential applications of the dataset**

307 Soils are integral to global biogeochemical cycles, directly influencing ecosystem productivity, nutrient
308 availability, and carbon storage. Understanding soil elemental composition and spatial variability is
309 essential for assessing ecosystem function and predicting responses to environmental changes (Schimel
310 et al., 2015). However, a persistent challenge in Earth system science has been the scarcity of high-
311 resolution, field-validated dataset, particularly in mountain regions where complex topography, diverse
312 vegetation, and steep climate gradients complicate both empirical and model-based analyses (Luo et al.,
313 2016b; Tito et al., 2020; Todd-Brown et al., 2013). This comprehensive, multi-element soil dataset fills
314 a critical data gap by providing spatially explicit measurements of 24 elements across 30 mountain
315 regions in China, spanning five major climatic zones and three soil development horizons. It offers unique
316 opportunities for a wide range of applications in Earth system science.

317 *Advancing biogeochemical modeling.* The dataset is well-suited for parameterizing, calibrating, and
318 validating a variety of biogeochemical models that simulate nutrient cycling, soil organic matter
319 dynamics, and element transport under changing environmental conditions. For instance, decomposition
320 models typically rely on the stoichiometry of carbon and nutrients, as well as interactions with
321 environmental drivers such as temperature, moisture, and pH (Fang et al., 2019; Feng and Zhu, 2021).
322 Our dataset provides detailed measurements of these variables across spatial and vertical gradients,
323 enabling more accurate estimation of model parameters that govern decomposition rates, mineralization,
324 and nutrient retention. The dataset also enables model validation through comparison between simulated
325 outputs and observed element concentrations in diverse mountain ecosystems. In addition, the inclusion

of horizon-specific data (O, A, and C horizons), weathering indices, and lithological information provides valuable input for soil formation and rock weathering models. Process-based models like SoilGen or conceptual frameworks such as CLORPT (climate, organisms, relief, parent material, and time) can benefit from the dataset's vertical resolution and environmental coverage to simulate pedogenesis, profile evolution, and mineral nutrient release across climate gradients. Accordingly, the dataset can serve as a regional benchmark for calibrating and validating long-term soil development models, particularly in mountainous regions where such data are scarce yet critically needed.

Enhancing soil quality assessment and ecosystem risk evaluation. Beyond modeling, the dataset provides a valuable reference for assessing soil quality and ecological risks in mountain regions. Measurements of SOC and macronutrient concentrations (e.g., P, K, and Ca) serve as indicators of soil fertility and ecosystem productivity (Bauters et al., 2022; Cunha et al., 2022; Rizzo et al., 2024). Simultaneously, the inclusion of micronutrients and trace elements enables evaluation of potential ecological hazards associated with heavy metal accumulation (Hou et al., 2025; Jin et al., 2024; Zhao et al., 2024). By capturing both beneficial and toxic elements, the dataset supports the identification of nutrient-deficient or polluted soils, informing the development of region-specific soil quality benchmarks. This is particularly relevant for mountainous ecosystems, where natural heterogeneity in soil properties can lead to localized environmental vulnerabilities. Furthermore, the dataset offers a foundation for integrated assessments of soil health and ecosystem services, including nutrient cycling efficiency, pollutant buffering capacity, and biodiversity support.

Supporting scenario analysis and climate adaptation planning. By linking elemental concentrations with environmental drivers (e.g., climate variables, vegetation indices, and soil chemical properties), this dataset enables predictive analyses of how soil function may shift under future environmental conditions. For instance, projections of climate change, altered precipitation regimes, or land-use intensification can be used to model potential changes in soil nutrient availability, carbon storage, and heavy metal mobility (Giovannelli et al. 2023; Ochoa-Hueso et al., 2023). These capabilities are essential for developing adaptive land management strategies aimed at enhancing soil resilience and ecosystem sustainability in vulnerable mountain regions.

Contributing to global soil and ecosystem monitoring initiatives. The dataset contributes to global efforts in soil monitoring and environmental data sharing, such as those led by the Global Soil Partnership

(GSP), the International Soil Reference and Information Centre (ISRIC), and global biogeochemical databases (e.g., SoilGrids, GEOTRACES) (Shi et al., 2025). Its high spatial resolution, standardized sampling protocols, and comprehensive coverage make it a valuable input for global-scale assessments of soil health, elemental cycling, and climate-soil-ecosystem interactions.

In summary, this dataset represents a significant advancement in the empirical foundation available for Earth system research in mountainous environments. It offers broad applicability for improving biogeochemical models, refining soil quality assessments, evaluating ecological risks, and informing sustainable land management and climate adaptation strategies. By enabling deeper understanding of soil processes across complex environmental gradients, this dataset contributes to ongoing efforts to conserve and manage mountain ecosystems in the face of accelerating global change.

5 Data availability

The database is freely accessible via the National Tibetan Plateau/Third Pole Environment Data Center at https://doi.org/10.11888/Terre.tpdc.302620 or https://cstr.cn/18406.11.Terre.tpdc.302620 (Wu et al., 2025b). The dataset provides comprehensive information for each sample, including mountain affiliation, geographical coordinates, climatic characteristics, vegetation type, soil type, parent rock type, normalized difference vegetation index, atmospheric nitrogen deposition rates, soil physicochemical properties, chemical weathering indices, and concentrations of 24 soil elements. The data are stored in Excel spreadsheet format, accompanied by a separate data documentation file that describes variable names, units, and definitions.

Author contributions

BHJ, WuYH, and ZG designed the experiments. BHJ and LJ sampled the soils, BHJ, WangYH, YWZ, and ZJ performed the analysis of soil samples. WYY, BHJ, and WangYH analyzed the data. WYY and BHJ wrote the first draft of the manuscript. WYY, BHJ, WangYH, YWZ, ZJ, WuYH, LJ, and ZG revised and improved the manuscript. All authors read and approved the final manuscript.

Competing interests

The contact author has declared that none of the authors has any competing interests.

Financial support

This study was supported by the Science and Technology Projects of Xizang Autonomous Region, China (XZ202501ZY0054), Sichuan Science and Technology Program (2024ZYD0038), the Science and

Technology Research Program of Institute of Mountain Hazards and Environment, Chinese Academy of Sciences (IMHE-ZDRW-06).

References

Agnan, Y., Courault, R., Alexis, M. A., Zanardo, T., Cohen, M., Sauvage, M., and Castrec-Rouelle, M.: Distribution of trace and major elements in subarctic ecosystem soils: Sources and influence of vegetation, Sci. Total Environ., 682, 650-662. https://doi.org/10.1016/j.scitotenv.2019.05.178, 2019.

Antonelli, A., Kissling, W., Flantua, S. G., Bermúdez, M. A., Mulch, A., Muellner-Riehl, A. N., Kreft, H., Linder, H. P., Badgley, C., Fjeldså, J., Fritz, S. A., Rahbek, C., Herman, F., Hooghiemstra, H., and Hoorn, C.: Geological and climatic influences on mountain biodiversity, Nat. Geosci., 11, 718-725, https://doi.org/10.1038/s41561-018-0236-z, 2018.

Augusto, L., Achat, D. L., Jonard, M., Vidal, D., and Ringeval, B.: Soil parent material—A major driver of plant nutrient limitations in terrestrial ecosystems, Global Change Biol., 23, 3808-3824, https://doi.org/10.1111/gcb.13691, 2017.

Barrow, N. J., and Hartemink, A. E.: The effects of pH on nutrient availability depend on both soils and plants, Plant Soil, 487, 21-37, https://doi.org/10.1007/s11104-023-05960-5, 2023.

Bauters, M., Janssens, I. A., Wasner, D., Doetterl, S., Vermeir, P., Griepentrog, M., Drake, T. W., Six, J., Barthel, M., Baumgartner, S., Van Oost, K., Makelele, I. A., Ewango, C. E., Verheyen, K., and Boeckx, P.: Increasing calcium scarcity along Afrotropical forest succession, Nat. Ecol. Evol., 6, 1122-1131, https://doi.org/10.1038/s41559-022-01810-2, 2022.

Bing, H. J., Qiu, S. J., Tian, X., Li, J., Zhu, H., Wu, Y. H., and Zhang, G.: Trace metal contamination in soils from mountain regions across China: Spatial distribution, sources, and potential drivers, Soil Ecol. Lett., 3, 189-206, https://doi.org/10.1007/s42832-021-0080-8, 2021.

Bing, H. J., Liu, Y., Huang, J. C., Tian, X., Zhu, H., and Wu, Y. H.: Dam construction attenuates trace metal contamination in water through increased sedimentation in the Three Gorges Reservoir, Water Res., 217, 118419, https://doi.org/10.1016/j.watres.2022.118419, 2022.

Bing, H. J., Wu, Y. H., Li, J., Xiang, Z. X., Luo, X. S., Zhou, J., Sun, H. Y., and Zhang, G.: Biomonitoring trace element contamination impacted by atmospheric deposition in China's remote mountains, Atmos. Res., 224, 30-41, https://doi.org/10.1016/j.atmosres.2019.03.018, 2019.

Bing, H. J., Wu, Y. J., Zhou, J., Li, R., Luo, J., and Yu, D.: Vegetation and cold trapping modulating

elevation-dependent distribution of trace metals in soils of a high mountain in Eastern Tibetan Plateau, Sci. Rep., 6, 24081, https://doi.org/10.1038/srep24081, 2016.

Cronan, C. S.: Soil Biogeochemistry, In: Ecosystem Biogeochemistry, Springer Textbooks in Earth Sciences, Geography and Environment, Springer, Cham, 11-29, https://doi.org/10.1007/978-3-319-66444-6_2, 2018.

Cui, Y. X., Bing, H. J., Moorhead, D. L., Delgado-Baquerizo, M., Ye, L. P., Yu, J. L., Zhang, S. P., Wang, X., Peng, S. S., Guo, X., Zhu, B., Chen, J., Tan, W. F., Wang, Y. Q., Zhang, X. C., and Fang, L. C.: Ecoenzymatic stoichiometry reveals widespread soil phosphorus limitation to microbial metabolism across Chinese forests, Commun. Earth Environ., 3, 184, https://doi.org/10.1038/s43247-022-00523-5, 2022.

Cunha, H. F., Andersen, K. M., Lugli, L. F., Santana, F. D., Aleixo, I. F., Moraes, A. M., Garcia, S., di Ponzio, R., Mendoza, E. O., Brum, B., Rosa, J. S., Cordeiro, A. L., Portela, B. T., Ribeiro, G., Coelho, S. D., de Souza, S. T., Silva, L. S., Antonieto, F., Pires, M. D., Salomão, A. C., Miron, A. C., de Assis, R. L., Domingues, T. F., Aragão, L. E., Meir, P., Camargo, J. L., Manzi, A. O., Nagy, L., Mercado, L. M., Hartley, I. P., and Quesada, C. A.: Direct evidence for phosphorus limitation on Amazon forest productivity, Nature, 608, 558-562, https://doi.org/10.1038/s41586-022-05085-2, 2022.

Dai, Z. M., Guo, X., Lin, J. H., Wang, X., He, D., Zeng, R. J., Meng, J., Luo, J. P., Delgado-Baquerizo, M., Moreno-Jiménez, E., Brookes, P.C., and Xu, J. M.: Metallic micronutrients are associated with the structure and function of the soil microbiome, Nat. Commun. 14, 8456, https://doi.org/10.1038/s41467-023-44182-2, 2023.

Dainese, M., Crepaz, H., Bottarin, R., Fontana, V., Guariento, E., Hilpold, A., Obojes, N., Paniccia, C., Scotti, A., Seeber, J., Steinwandter, M., Tappeiner, U., and Niedrist, G.: Global change experiments in mountain ecosystems: A systematic review, Ecol. Monogr., 94, e1632, https://doi.org/10.1002/ecm.1632, 2024.

Elser, J. J., Fagan, W. F., Kerkhoff, A. J., Swenson, N. G., and Enquist, B. J.: Biological stoichiometry of plant production: metabolism, scaling and ecological response to global change, New Phytol., 186, 593-608, https://doi.org/10.1111/j.1469-8137.2010.03214.x, 2010.

Fang, X. M., Zhang, X. L., Chen, F. S., Zong, Y. J., Bu, W. S., Wan, S. Z., Luo, Y. Q., and Wang, H. M.:

Phosphorus addition alters the response of soil organic carbon decomposition to nitrogen deposition in a subtropical forest, Soil Biol. Biochem., 133, 119-128, https://doi.org/10.1016/j.soilbio.2019.03.005, 2019.

Feng, J. G., and Zhu, B.: Global patterns and associated drivers of priming effect in response to nutrient addition, Soil Biol. Biochem., 153, 108118, https://doi.org/10.1016/j.soilbio.2020.108118, 2021.

Feng, W., Mariotte, P., Gu, J., Song, X., Yang, J., Yang, F., Zhao, Y., and Zhang, G.: Impacts of geography, climate, soil properties and vegetation characteristics on soil C:N:P stoichiometry across the Qinghai-Tibetan Plateau, Pedosphere, https://doi.org/10.1016/j.pedsph.2024.06.012, 2024.

Fernández-Martínez, M.: From atoms to ecosystems: Elementome diversity meets ecosystem functioning, New Phytol., 234: 35-42, https://doi.org/10.1111/nph.17864, 2021.

Giovannelli, D.: Trace metal availability and the evolution of biogeochemistry, Nat. Rev. Earth Environ., 4, 597-598, https://doi.org/10.1038/s43017-023-00477-y, 2023.

Haghverdi, K., and Kooch, Y.: Effects of diversity of tree species on nutrient cycling and soil-related processes, Catena, 178, 335-344, https://doi.org/10.1016/j.catena.2019.03.041, 2019.

Han W. X., Fang J. Y., Reich, P. B., Woodward, F. I., and Wang, Z. H.: Biogeography and variability of eleven mineral elements in plant leaves across gradients of climate, soil and plant functional type in China, Ecol. Lett., 14, 788-796, https://doi.org/10.1111/j.1461-0248.2011.01641.x, 2011.

Hay Mele, B., Monticelli, M., Leone, S., Bastoni, D., Barosa, B., Cascone, M., Migliaccio, F., Montemagno, F., Ricciardelli, A., Tonietti, L., Rotundi, A., Cordone, A., and Giovannelli, D.: Oxidoreductases and metal cofactors in the functioning of the earth, Essays Biochem., 67, 653-670, https://doi.org/10.1042/EBC20230012, 2023.

Hou, D. Y., Jia, X. Y., Wang, L. W., McGrath, S. P., Zhu, Y. G., Hu, Q., Zhao, F. J., Bank, M. S., O'Connor, D., and Nriagu, J.: Global soil pollution by toxic metals threatens agriculture and human health, Science, 388(6744), 316-321, https://doi.org/10.1126/science.adr5214, 2025.

IPCC: Climate Change 2021: The Physical Science Basis. Cambridge University Press, Cambridge, UK, 2021.

Jin, J. Y., Zhao, D. Y., Wang, J. P., Wang, Y. H., Zhu, H., Wu, Y. H., Fang, L. C., and Bing, H. J.: Fungal community determines soil multifunctionality during vegetation restoration in metallic tailing reservoir, J. Hazard Mater., 478, 135438, https://doi.org/10.1016/j.jhazmat.2024.135438, 2024.

Jobbágy, E. G., and Jackson, R. B.: The distribution of soil nutrients with depth: Global patterns and the imprint of plants, Biogeochemistry, 53, 51-77, https://doi.org/10.1023/A:1010760720215, 2001.

Jobbágy, E. G., and Jackson, R. B.: The uplift of soil nutrients by plants: Biogeochemical consequences across scales, Ecology, 85, 2380-2389, https://doi.org/10.1890/03-0245, 2004.

Kaspari, M. and Powers, J. S.: Biogeochemistry and geographical ecology: Embracing all twenty-five elements required to build organisms, Am. Nat., 188, 62-73, https://doi.org/10.1086/687576, 2016.

Kirkby, M. J.: A conceptual model for physical and chemical soil profile evolution, Geoderma, 331, 121-130, https://doi.org/10.1016/j.geoderma.2018.06.009, 2018.

Kou, Y. P., Zhao, W. Q., Liu, Y. J., Wu, Y. H., Xiao, J. T., Wang, X. H., Bing, H. J., and Liu, Q.: Diversity patterns and drivers of methanotrophic gene distributions in forest soils across a large latitudinal gradient, Glob. Ecol. Biogeogr., 30, 2004-2015, https://doi.org/10.1111/geb.13362, 2021.

Lu, L. M., Mao, L. F., Yang, T., Ye, J. F., Liu, B., Li, H. L., Sun, M., Miller, J. T., Mathews, S., Hu, H. H., Niu, Y. T., Peng, D. X., Chen, Y. H., Smith, S. A., Chen, M., Xiang, K. L., Le, C. T., Dang, V. C., Lu, A. M., Soltis, P. S., Soltis, D. E., Li, J. H., and Chen, Z. D.: Evolutionary history of the angiosperm flora of China, Nature, 554, 234-238, https://doi.org/10.1038/nature25485, 2018.

Luo, W., Sardans, J., Dijkstra, F. A., Peñuelas, J., Lü, X. T., Wu, H., Li, M. H., Bai, E., Wang, Z., Han, X. and Jiang, Y.: Thresholds in decoupled soil-plant elements under changing climatic conditions, Plant Soil, 409, 159-173, https://doi.org/10.1007/s11104-016-2955-5, 2016a.

Luo, Y., Ahlström, A., Allison, S., Batjes, N., Brovkin, V., Carvalhais, N., Chappell, A., Ciais, P., Davidson, E., Finzi, A., Georgiou, K., Guenet, B., Hararuk, O., Harden, J., He, Y., Hopkins, F., Jiang, L., Koven, C., Jackson, R., Jones, C. D., Lara, M. J., Liang, J., McGuire, A. D., Parton, W., Peng, C., Randerson, J. T., Salazar, A., Sierra, C. A., Smith, M. J., Tian, H., Todd-Brown, K. E. O., Torn, M., van Groenigen, K. J., Wang, Y. P., West, T. O., Wei, Y., Wieder, W. R., Xia, J., Xu, X., Xu, X. F., Zhou, T.: Toward more realistic projections of soil carbon dynamics by Earth system models, Global Biogeochem. Cy., 30, 40-56, https://doi.org/10.1002/2015GB005239, 2016b.

Lynch, J. P., and St. Clair, S. B.: Mineral stress: The missing link in understanding how global climate change will affect plants in real world soils, Field Crops Res., 90, 101-115, https://doi.org/10.1016/j.fcr.2004.07.008, 2004.

Maynard, D. G., and Curran, M. P.: Bulk density measurement in forest soils, Soil sampling and methods

of analysis, 863-869, https://doi.org/10.1201/978142000527, 2007.

McLennan, S. M.: Weathering and Global Denudation, J. Geol., 101, 295-303, https://doi.org/10.1086/648222, 1993.

Molina, A., Vanacker, V., Chadwick, O., Zhiminaicela, S., Corre, M. D., and Veldkamp, E.: Vegetation patterns associated with nutrient availability and supply in high-elevation tropical Andean ecosystems, Biogeosciences, 21, 3075-3091, https://doi.org/10.5194/bg-21-3075-2024, 2024.

Moreno-Jiménez, E., Maestre, F. T., Flagmeier, M., Guirado, E., Berdugo, M., Bastida, F., Dacal, M., Díaz-Martínez, P., Ochoa-Hueso, R., Plaza, C., Rillig, M. C., Crowther, T. W., and Delgado-Baquerizo, M.: Soils in warmer and less developed countries have less micronutrients globally, Global Change Biol., 29, 522-532, https://doi.org/10.1111/gcb.16478, 2022.

Moreno-Jiménez, E., Plaza, C., Saiz, H., Manzano, R., Flagmeier, M., and Maestre, F. T.: Aridity and reduced soil micronutrient availability in global drylands, Nat. Sustain., 2, 371-377, https://doi.org/10.1038/s41893-019-0262-x, 2019.

Nagajyoti, P. C., Lee, K. D. and Sreekanth, T. V. M.: Heavy metals, occurrence and toxicity for plants: A review, Environ. Chem. Lett., 8, 199-216, https://doi.org/10.1007/s10311-010-0297-8, 2010.

Nesbitt, H. W., and Young, G. M.: Early Proterozoic climates and plate motions inferred from major element chemistry of lutites, Nature, 299, 715-717, https://doi.org/10.1038/299715a0, 1982.

Nogués-Bravo, D., Araújo, M. B., Errea, M. P., and Martínez-Rica, J. P.: Exposure of global mountain systems to climate warming during the 21st Century, Global Environ. Chang., 17, 420-428, https://doi.org/10.1016/j.gloenvcha.2006.11.007, 2007.

Ochoa-Hueso, R., Delgado-Baquerizo, M., Risch, A. C., Ashton, L., Augustine, D., Bélanger, N., Bridgham, S., Britton, A. J., Bruckman, V. J., Camarero, J. J., Cornelissen, G., Crawford, J. A., Dijkstra, F. A., Diochon, A., Earl, S., Edgerley, J., Epstein, H., Felton, A., Fortier, J., Gagnon, D., Greer, K., Griffiths, H. M., Halde, C., Hanslin, H. M., Harris, L. I., Hartsock, J. A., Hendrickson, P., Hovstad, K. A., Hu, J., Jani, A. D., Kent, K., Kerdraon-Byrne, D., Khalsa, S. D. S., Lai, D. Y. F., Lambert, F., LaMontagne, J. M., Lavergne, S., Lawrence, B. A., Littke, K., Leeper, A. C., Licht, M. A., Liebig, M. A., Lynn, J. S., Maclean, J. E., Martinsen, V., McDaniel, M. D., McIntosh, A. C. S., Miesel, J. R., Miller, J., Mulvaney, M. J., Moreno, G., Newstead, L., Pakeman, R. J., Pergl, J., Pinno, B. D., Piñeiro, J., Quigley, K., Radtke, T. M., Reed, P., Rolo, V., Rudgers, J., Rutherford, P. M.,

Sayer, E. J., Serrano-Grijalva, L., Strack, M., Sukdeo, N., Taylor, A. F. S., Truax, B., Tsuji, L. J. S., van, G., Vaness, B. M., Van, S., Vítková, M., Weigel, R., Wilton, M. J., Yano, Y., Teen, E., and Bremer, E.: Bioavailability of macro and micronutrients across global topsoils: Main drivers and global change impacts, Global Biogeochem. Cy., 37, e2022GB007680, https://doi.org/10.1029/2022GB007680, 2023.

Peñuelas, J., Fernández-Martínez, M., Ciais, P., Jou, D., Piao, S. L., Obersteiner, M., Vicca, S., Janssens, I. A., and Sardans, J.: The bioelements, the elementome, and the biogeochemical niche, Ecology, 100, e02652, https://doi.org/10.1002/ecy.2652, 2019.

Ren, H., Zhou, Q., He, J., Hou, Y., Jiang, Y., Rodrigues, J. L. M., Cobb, A. B., Wilson, G. W. T., Hu, J., and Zhang, Y.: Determining landscape-level drivers of variability for over fifty soil chemical elements, Sci. Total Environ., 657, 279-286, https://doi.org/10.1016/j.scitotenv.2018.12.024, 2019.

Rizzo, G., Agus, F., Susanti, Z., Buresh, R., Cassman, K. G., Dobermann, A., Agustiani, N., Aristya, V. E., Batubara, S. F., Istiqomah, N., Oberthür, T., Pasuquin, J. M., Samijan, Witt, C., and Grassini, P.: Potassium limits productivity in intensive cereal cropping systems in Southeast Asia, Nat. Food 5, 929-938, https://doi.org/10.1038/s43016-024-01065-z, 2024.

Sayer, E. J., Rodtassana, C., Sheldrake, M., Sheldrake, M., Bréchet, L. M., Ashford, O. S., Lopez-Sangil, L., Kerdraon-Byrne, D., Castro, B., Turner, B. L., Wright, S. J., and Tanner, E. V.: Revisiting nutrient cycling by litterfall -- Insights from 15 years of litter manipulation in old-growth lowland tropical forest, Adv. Ecol. Res., 62, 173-223, https://doi.org/10.1016/bs.aecr.2020.01.002, 2020.

Schimel, D. S., Pavlick, R. P., Fisher, J. B., Asner, G. P., Saatchi, S. S., Townsend, P. A., Miller, C. E., Frankenberg, C., Hibbard, K. A., and Cox, P. M.: Observing terrestrial ecosystems and the carbon cycle from space, Global Change Biol., 21(5), 1762-1776, https://doi.org/10.1111/gcb.12822, 2015.

Shafiee, R. T., Diver, P., Snow, J. T., Zhang, Q., and Rickaby, R. E.: Marine ammonia-oxidising archaea and bacteria occupy distinct iron and copper niches, ISME Commun., 1, https://doi.org/10.1038/s43705-021-00001-7, 2021.

Shangguan, W., Dai, Y., Duan, Q., Liu, B., and Yuan, H.: A global soil data set for Earth system modeling, J. Adv. Model. Earth Syst., 6(1), 249-263, https://doi.org/10.1002/2013MS000293, 2014.

Shi, G. S., Sun, W. Y., Wei, S. G., Wei, Z. W., Yuan, H., Li, L., Sun, X. L., Zhang, Y. Liang, H. B., Li, D. X., Huang, F. N., Li, Q. L., Dai, Y. J.: A China dataset of soil properties for land surface modeling

(version 2), Earth Syst. Sci. Data, 17, 517-543, https://doi.org/10.5194/essd-17-517-2025, 2025.

Steinnes, E., and Lierhagen, S.: Geographical distribution of trace elements in natural surface soils: Atmospheric influence from natural and anthropogenic sources, Appl. Geochem., 88, 2-9, https://doi.org/10.1016/j.apgeochem.2017.03.013, 2018.

Sundqvist, M. K., Sanders, N. J. and Wardle, D. A.: Community and ecosystem responses to elevational gradients: processes, mechanisms and insights for global change, Annu. Rev. Ecol. Evol. S., 44, 261-280, https://doi.org/10.1146/annurev-ecolsys-110512-135750, 2013.

Tian, D., Reich, P. B., Chen, H. Y. H., Xiang, Y., Luo, Y., Shen, Y., Meng, C., Han, W., and Niu, S.: Global changes alter plant multi-element stoichiometric coupling, New Phytol., 221(2), 807-817, https://doi.org/10.1111/nph.15428, 2019.

Tito, R., Vasconcelos, H. L., and Feeley, K. J.: Mountain ecosystems as natural laboratories for climate change experiments, Front. For. Glob. Change, 3, https://doi.org/10.3389/ffgc.2020.00038, 2020.

Todd-Brown, K. E., Randerson, J. T., Post, W. M., Hoffman, F. M., Tarnócai, C., Schuur, E. A., and Allison, S. D.: Causes of variation in soil carbon simulations from CMIP5 Earth system models and comparison with observations, Biogeosciences, 10, 1717-1736, https://doi.org/10.5194/bg-10-1717-2013, 2013.

Vallicrosa, H.: Beyond nitrogen and phosphorus, Nat. Ecol. Evol., 6, 1056-1057, https://doi.org/10.1038/s41559-022-01788-x, 2022.

Wang, J., Hu, A., Meng, F., Zhao, W., Yang, Y., Soininen, J., Shen, J., and Zhou, J.: Embracing mountain microbiome and ecosystem functions under global change, New Phytol., 234, 1987-2002, https://doi.org/10.1111/nph.18051, 2022.

Wang, Y., Bing, H., Moorhead, D. L., Hou, E., Wu, Y., Wang, J., Duan, C., Cui, Q., Zhang, Z., and Zhu, H.: Bacterial community structure modulates soil phosphorus turnover at early stages of primary succession, Global Biogeochem. Cy., 38, e2024GB008174, https://doi.org/10.1029/2024GB008174, 2024.

Woodruff, L. G., Cannon, W. F., Eberl, D. D., Smith, D. B., Kilburn, J. E., Horton, J. D., Garrett, R. G., and Klassen, R. A.: Continental-scale patterns in soil geochemistry and mineralogy: Results from two transects across the United States and Canada, Appl. Geochem., 24, 1369-1381, https://doi.org/10.1016/j.apgeochem.2009.04.009, 2009.

Wu, Y. Y., Wang, Y. H., Ochoa-Hueso, R., Hou, E. Q., Li, J., Zhu, H., Sardans, J., Fang, L. C., Wu, Y. H., Zhang, G., Peñuelas, J., and Bing, H. J.: From bedrock to life activity and atmospheric deposition: Drivers of soil element coupling across horizons, Environ. Res., 271, 121070, https://doi.org/10.1016/j.envres.2025.121070, 2025a.

Wu, Y. Y., Bing, H. J., Wang, Y. H., Yang, W. Z., Zhang, J., Wu, Y. H., Li, J., and Zhang, G.: Multi-element dataset across diverse climatic zones and soil profiles in China's mountains, National Tibetan Plateau/Third Pole Environment Data Center, https://doi.org/10.11888/Terre.tpdc.302620, 2025b.

Yang, W. Z., Bing, H. J., Tian, X., Liu, Y., Zhu, H., Fang, L. C., and Wu, Y. H.: Unearthing the importance of soil development in total phosphorus distribution in China's mountains, Catena, 228, 107193, https://doi.org/10.2139/ssrn.4357696, 2023.

Yang, Z. J., Bing, H. J., Zhou, J., Wu, Y. H., Sun, H. Y., Luo, J., Sun, S. Q., and Wang, J. P.: Variation of mineral composition along the soil chronosequence at the Hailuogou Glacier foreland of Gongga Mountain, Acta Pedol. Sin., 52, 507-516, https://doi.org/10.11766/trxb201406180301, 2015.

Yu, G. R., Jia, Y. L., He, N. P., Zhu, J. X., Chen, Z., Wang, Q. F., Piao, S. L., Liu, X. J., He, H. L., Guo, X. B., Wen, Z., Li, P., Ding, G. A., and Goulding, K.: Stabilization of atmospheric nitrogen deposition in China over the past decade, Nat. Geosci., 12, 424-429, https://doi.org/10.1038/s41561-019-0352-4, 2019.

Zhao, D., Bol, R., Wang, J., Jin, J., Wang, Y., Wang, T., Zhu, H., Wu, Y., Fang, L., and Bing, H.: Soil heavy metal pollution promotes extracellular enzyme production by mediating microbial community structure during vegetation restoration of metallic tailing reservoir, Sci. Total Environ., 948, 174783, https://doi.org/10.1016/j.scitotenv.2024.174783, 2024.

Zhao, W. Q., Kou, Y. P., Wang, X. H., Wu, Y. H., Bing, H. J., and Liu, Q.: Broad-scale distribution of diazotrophic communities is driven more by aridity index and temperature than by soil properties across various forests, Glob. Ecol. Biogeogr., 29, 2119-2130, https://doi.org/10.1111/geb.13178, 2020.

Zhi, X. C., Jin, Y. B., Meng, Q., and Gao, T. S.: Trace element geochemistry of Raobazhai ultramafic complex, North Dabie Mountain, Acta Petrol. Sin., 20, 463-472, 2004.

Zomer, R. J., Xu, J., and Trabucco, A.: Version 3 of the global aridity index and potential

evapotranspiration database, Sci. Data, 9, 409, https://doi.org/10.1038/s41597-022-01493-1, 2022.

Zuo, Z. J., Reich, P. B., Qiao, X. J., Zhao, H. C., Zhang, L. J., Yang, L., Lv, T., Tang, Z. Y., Yu, D., and Wang, Z.: Coordination between bioelements induce more stable macroelements than microelements in wetland plants. Ecol. Lett., 27, e70025, https://doi.org/10.1111/ele.70025, 2024.

620 **Figure legends**

621 **Fig. 1** Geographic distribution of the 30 China's mountains. AL, Mt. Ailao; AS, Mt. Ao; BCW, Mt.
622 Baicaowa; CB, Mt. Changbai; DB, Mt. Dabie; DH, Mt. Dinghu; DX, Mt. Daxinganling; DYS, Mt.
623 Daiyun; FJS, Mt. Fanjing; GD, Mt. Guandi; GGS, Mt. Gongga; HS, Mt. Han; JF, Mt. Jifeng; JG, Mt.
624 Jiugong; JGS, Mt. Jinggang; LJ, Mt. Luoji; LG, Mt. Leigong; ME, Mt. Maoer; NL, Mt. Nanling; QF, Mt.
625 Qingfengxia; QL, Mt. Qinling; SHB, Mt. Saihanba; SN, Mt. Shennongjia; SWDS, Mt. Shiwandashan;
626 SYK, Mt. Suyukou; TM, Mt. Tianmu; WGS, Mt. Wugong; WYZ, Mt. Wuyuezhai; WZS, Mt. Wuzhi; XX,
627 Mt. Xiaoxinganling.

628 **Fig. 2** Frequency distribution of soil elements across the China's mountains. Red curve on each histogram
629 represents the fitted normal distribution. The statistical parameters of the corresponding element are
630 annotated in the upper left of each sub-figure.

631 **Fig. 3** Mean concentrations of 24 elements across different soil horizons. Lowercase letters indicate
632 significant differences in each element among soil horizons ($p < 0.05$), and error bars represent the
633 standard error.

634 **Fig. 4** Spatial distribution of soil element concentrations across latitude, longitude, and altitude. The
635 colors of the dots represent different soil horizons. Solid red lines represent the fitting relationships of
636 elemental concentrations with latitude, longitude, and altitude ($p<0.05$). R^2 less than 0.05 are not shown.

637 **Fig. 5** The environmental factors influencing the elemental concentrations in the soils. (a) Redundancy
638 analysis (RDA) shows the relationships of soil elements with environmental factors across soil horizons.
639 The inserted figure shows the distribution of samples along the axes. (b) Correlation heatmap shows the
640 correlation between soil element concentrations and environmental variables in each soil horizon. The
641 color and circle size represent the correlation coefficient, and * indicates statistical significance ($p < 0.05$).
642 SOC, soil organic carbon; MAP, mean annual precipitation; MAT, mean annual temperature; AI, aridity
643 index; NDVI, normalized difference vegetation index; BD, bulk density; CIA, chemical index of
644 alteration

645 **Fig. 6** Effects of environmental factors on elemental variability based on random forest models. The bar
646 plots show the proportion of variance explained for individual elements. The heat maps depict the relative
647 importance of environmental factors in predicting elemental variability, with darker shades indicating
648 greater importance. MAP, mean annual precipitation; MAT, mean annual temperature; AI, aridity index;

649 NDVI, normalized difference vegetation index; CIA, chemical index of alteration.

650 **Table1** The basic information across China's mountains (n =30)

Climatic zone	Mountain ID	n	Latitude (°N)	Longitude (°E)	Altitude (m)	MAP (mm)	MAT (°C)	Vegetation types
Cold-temperate	DX	133	49.25-53.45	122.34-124.28	360-1370	514	-3.1	Broadleaf forest, Coniferous-broadleaf mixed forest, Coniferous forest
	BCW	36	40.82-40.83	117.60-117.61	1120-1710	539	6.0	Coniferous forest
	CB	58	42.06-42.30	127.83-128.13	1025-2000	828	-1.0	Broadleaf forest, Coniferous forest
	HS	51	44.19-44.27	118.41-118.72	1100-1400	400	1.0	Broadleaf forest, Coniferous-broadleaf mixed forest, Coniferous forest
Temperate	ME	12	45.39-45.39	127.68-127.68	400-400	599	2.7	Coniferous-broadleaf mixed forest
	SHB	36	42.33-42.47	117.29-117.51	1560-1870	452	1.0	Broadleaf forest, Coniferous-broadleaf mixed forest
	SYK	27	38.73-38.75	105.91-105.92	2030-2350	243	4.3	Coniferous forest
	XX	78	46.63-48.85	128.47-129.65	240-1420	639	0.2	Broadleaf forest, Coniferous-broadleaf mixed forest
	AS	84	33.79-33.96	107.30-107.50	1260-3150	786	6.2	Broadleaf forest, Coniferous-broadleaf mixed forest, Coniferous forest
	GD	42	37.89-37.90	111.43-111.44	1310-2200	5211	2.4	Broadleaf forest, Coniferous-broadleaf mixed forest, Coniferous forest, Shrub
Warm-temperate	JF	18	33.68-33.69	105.68-105.68	1785-1900	670	12.2	Coniferous forest
	QF	27	34.00-34.04	107.44-107.44	1530-2100	737	7.6	Broadleaf forest, Coniferous-broadleaf mixed forest
	QL	66	34.02-34.16	107.61-107.80	870-2350	750	6.4	Broadleaf forest, Coniferous-broadleaf mixed forest, Coniferous forest
	WYZ	42	38.72-38.73	113.84-113.86	1210-1880	476	6.9	Broadleaf forest, Coniferous-broadleaf mixed forest,

								Coniferous forest, Shrub
	AL	45	24.50-24.54	100.99-101.03	2190-2655	971	14.1	Broadleaf forest, Coniferous-broadleaf mixed forest
	DB	45	31.09-31.10	115.77-115.81	400-1630	1562	11.4	Coniferous-broadleaf mixed forest, Coniferous forest
	DH	27	23.17-23.18	112.52-112.54	210-586	1788	21.1	Coniferous-broadleaf mixed forest
	DYS	30	25.64-25.65	118.22-118.22	1100-1510	1546	15.9	Coniferous-broadleaf mixed forest, Coniferous forest
	FJS	19	27.90-27.91	108.70-108.72	1482-2095	1346	11.6	Broadleaf forest
	GGS	66	29.54-29.60	101.96-102.07	2000-4225	967	6.6	Broadleaf forest, Coniferous forest, Shrub
	JG	27	29.38-29.40	114.58-114.62	580-1230	1635	13.8	Coniferous-broadleaf mixed forest, Coniferous forest
Subtropical	JGS	30	26.51-26.63	114.11-114.17	925-1350	1727	14.0	Coniferous-broadleaf mixed forest
	LG	24	26.36-26.38	108.16-108.21	1223-2155	1294	12.6	Broadleaf forest, Coniferous forest, Shrub
	LJ	51	27.57-27.58	102.37-102.42	2200-3830	940	7.5	Broadleaf forest, Coniferous forest
	NL	18	24.90-24.95	112.99-113.05	800-1545	1700	14.9	Broadleaf forest, Coniferous-broadleaf mixed forest, Coniferous forest
	SN	105	31.36-31.76	110.15-110.55	1110-3090	1274	7.7	Broadleaf forest, Coniferous-broadleaf mixed forest, Coniferous forest
	SWDS	45	21.88-21.90	107.90-107.92	393-708	1908	20.0	Broadleaf forest, Coniferous-broadleaf mixed forest
	TM	21	30.36-30.58	119.43-119.73	790-1460	1382	14.0	Coniferous-broadleaf mixed forest
	WGS	27	27.46-27.46	114.16-114.17	778-1175	1767	13.6	Broadleaf forest
Tropical	WZS	24	18.89-18.90	109.69-109.71	862-1818	1694	20.8	Broadleaf forest

651 AL, Mt. Ailao; AS, Mt. Ao; BCW, Mt. Baicaowa; CB, Mt. Changbai; DB, Mt. Dabie; DH, Mt.

652 Dinghu; DX, Mt. Daxinganling; DYS, Mt. Daiyun; FJS, Mt. Fanjing; GD, Mt. Guandi; GGS, Mt.
653 Gongga; HS, Mt. Han; JF, Mt. Jifeng; JG, Mt. Jiugong; JGS, Mt. Jinggang; LJ, Mt. Luoji; LG, Mt.
654 Leigong; ME, Mt. Maoer; NL, Mt. Nanling; QF, Mt. Qingfengxia; QL, Mt. Qinling; SHB, Mt.
655 Saihanba; SN, Mt. Shennongjia; SWDS, Mt. Shiwandashan; SYK, Mt. Suyukou; TM, Mt. Tianmu;
656 WGS, Mt. Wugong; WYZ, Mt. Wuyuezhai; WZS, Mt. Wuzhi; XX, Mt. Xiaoxinganling; MAP, mean
657 annual precipitation; MAT, mean annual temperature.

658 **Table 2** The basic soil properties across the mountains (n =30)

Climatic zone	Mountain ID	Horizon	BD (g/cm^3)	Moisture (%)	pH	CIA
Cold-temperate	DX	O	0.11-0.21	70.0-182.2	3.37-6.73	53.40-67.58
		A	0.19-0.70	14.6-118.9	3.10-6.47	57.73-74.10
		C	0.50-1.39	9.1-44.6	3.70-6.44	57.6-74.04
	BCW	O	0.16-0.22	27.3-63.2	4.34-6.66	51.21-63.35
		A	0.24-0.59	25.4-37.5	4.88-6.54	53.82-62.86
		C	0.75-0.93	12.6-27.8	5.69-7.40	51.73-66.02
	CB	O	0.11-0.15	103.8-224.5	4.83-6.32	46.31-62.36
		A	0.18-0.31	86.2-152.0	4.34-6.44	49.90-62.77
		C	0.51-0.99	15.2-72.8	4.56-5.61	45.79-66.87
	HS	O	0.21-0.26	19.2-48.3	5.51-6.82	53.33-58.89
		A	0.32-0.70	18.3-27.0	5.16-6.62	53.11-58.54
		C	0.78-0.90	8.2-17.9	5.68-6.61	55.61-60.66
Temperate	ME	O	0.16-0.16	59.1-59.1	4.72-5.88	58.78-62.16
		A	0.38-0.38	42.0-42.0	4.49-5.24	58.08-61.88
		C	0.72-0.72	23.6-23.6	5.42-5.60	63.06-71.75
	SHB	O	0.16-0.23	25.0-66.9	5.70-7.08	58.82-62.28
		A	0.32-0.59	13.8-50.3	5.54-6.71	55.79-62.44
		C	0.84-0.92	7.5-22.0	5.36-6.44	57.28-61.71
	SYK	O	0.21-0.21	45.9-46.7	7.23-7.77	59.33-61.05
		A	0.25-0.36	34.9-45.6	7.28-7.92	58.76-59.95
		C	0.58-1.08	6.1-22.3	7.74-8.16	58.68-61.38
	XX	O	0.11-0.19	35.6-109.6	4.64-6.35	58.92-63.85
		A	0.30-0.54	30.5-60.1	4.11-6.09	57.78-66.81
		C	0.71-1.10	7.9-42.2	4.88-6.06	54.11-70.48
	AS	O	0.19-0.56	61.6-237.3	3.70-6.32	59.18-68.21
		A	0.24-0.63	45.9-204.9	4.05-6.63	57.08-70.85
		C	0.56-1.22	19.4-61.6	4.65-6.36	57.49-73.19
	GD	O	0.13-0.20	131.2-152.1	5.41-6.67	58.72-63.30
		A	0.25-0.59	61.1-127.3	5.63-6.72	57.39-59.84
		C	0.67-1.08	22.2-47.5	6.30-7.15	56.53-62.16
	JF	O	0.22-1.15	24.0-94.4	4.18-6.31	66.41-69.56
		A	0.21-0.55	40.0-180.0	4.27-5.40	66.71-70.03
		C	0.73-1.02	10.6-35.8	5.48-6.30	68.69-76.31
Warm-temperate	QF	O	0.17-0.22	113.0-139.6	5.74-6.44	47.61-65.72
		A	0.35-0.39	68.8-107.8	5.55-6.25	49.23-66.06
		C	0.59-0.88	30.2-47.3	5.96-6.41	49.89-65.65
	QL	O	0.16-0.30	73.4-173.6	5.55-7.22	59.04-64.97
		A	0.32-0.45	36.4-100.5	5.40-7.56	57.68-63.42
		C	0.73-1.20	8.1-37.5	5.60-8.11	50.17-64.64
	WYZ	O	0.11-0.18	116.9-145.7	4.12-7.07	58.90-64.72
		A	0.17-0.72	32.7-110.6	4.70-6.96	57.93-62.94
		C	0.77-0.96	15.3-22.3	5.81-6.33	60.68-66.56

		O	0.16-0.56	21.2-107.0	3.63-5.45	79.8-89.31
	AL	A	0.41-0.63	29.7-59.7	3.80-5.49	80.58-89.80
		C	0.69-0.92	24.8-45.7	4.55-5.53	79.87-91.00
		O	0.15-0.33	46.0-126.9	3.74-5.60	50.87-61.82
	DB	A	0.20-0.64	18.0-105.7	3.69-5.86	51.43-62.79
		C	0.82-1.03	8.5-26.2	4.66-5.90	51.45-74.48
		O	0.48-0.81	22.9-32.7	3.65-4.12	79.12-84.73
	DH	A	0.73-0.94	23.1-31.4	3.76-4.18	79.2-85.67
		C	0.88-1.15	15.5-17.9	3.97-4.32	79.95-85.76
	DYS	A	0.26-0.63	54.6-82.8	3.25-4.26	70.81-88.59
		C	0.53-0.97	32.4-49.4	3.58-4.31	77.30-89.18
		O	0.18-0.47	79.0-213.0	3.93-4.74	78.79-90.99
	FJS	A	0.24-0.40	66.3-197.0	4.06-4.73	79.95-92.02
		C	0.54-0.66	59.8-84.1	4.28-4.86	80.67-94.26
		O	0.15-0.24	58.5-73.1	3.39-6.76	52.55-63.91
	GGS	A	0.55-0.81	26.5-42.6	3.63-7.19	52.82-72.65
		C	1.11-1.30	13.4-29.4	4.28-8.02	48.12-75.17
		O	0.16-0.22	77.3-129.0	3.45-4.36	59.53-75.81
	JG	A	0.37-0.75	18.7-46.1	3.62-5.11	60.67-73.54
		C	0.68-0.89	14.6-19.1	4.36-5.22	55.5-74.38
	JGS	A	0.30-0.77	51.4-191.7	3.19-4.93	78.9-88.92
Subtropical		C	0.75-1.66	22.1-53.6	3.92-4.76	80.07-90.10
		O	0.43-0.48	77.5-78.9	4.11-4.67	76.37-86.52
	LG	A	0.49-0.74	18.8-70.3	4.26-4.71	79.38-87.29
		C	0.82-0.89	29.8-37.2	4.58-4.84	81.52-88.71
		O	0.18-0.36	74.5-173.1	3.59-3.91	54.95-69.98
	LJ	A	0.21-0.59	28.3-131.7	3.72-5.80	58.03-81.09
		C	0.85-1.02	19.5-40.1	3.83-6.34	59.00-82.45
		O	0.18-0.79	44.7-227.6	3.68-4.76	64.69-79.82
	NL	A	0.45-0.85	40.8-109.4	3.49-4.46	64.97-80.51
		C	0.83-1.12	14.7-43.5	4.12-4.61	66.8-83.91
		O	0.11-0.56	31.73-187.5	4.13-6.58	65.22-74.39
	SN	A	0.22-0.63	33.5-136.2	3.67-7.35	64.35-76.16
		C	0.55-0.96	20.5-61.3	4.16-6.78	68.13-81.39
		O	0.31-0.67	42.9-130.7	3.62-5.78	80.43-94.92
	SWDS	A	0.65-0.97	18.3-85.6	3.33-7.16	80.44-95.64
		C	0.84-1.52	17.3-41.0	3.69-4.28	80.69-95.81
		O	0.36-0.66	50.3-86.4	3.80-5.93	69.04-81.79
	TM	A	0.64-0.66	49.1-70.6	3.71-4.77	72.74-82.35
		C	0.92-0.92	29.9-29.9	4.58-4.66	74.97-75.77
	WGS	A	0.40-0.92	53.3-118.8	3.95-5.34	73.34-87.58
		C	0.55-1.00	37.6-101.5	3.90-5.67	70.28-87.65
	WZS	A	0.71-0.86	49.7-73.7	3.52-3.96	84.89-92.80
Tropical		C	1.04-1.38	25.2-32.2	3.98-4.42	85.40-93.40

AL, Mt. Ailao; AS, Mt. Ao; BCW, Mt. Baicaowa; CB, Mt. Changbai; DB, Mt. Dabie; DH, Mt. Dinghu; DX, Mt. Daxinganling; DYS, Mt. Daiyun; FJS, Mt. Fanjing; GD, Mt. Guandi; GGS, Mt. Gongga; HS, Mt. Han; JF, Mt. Jifeng; JG, Mt. Jiugong; JGS, Mt. Jinggang; LJ, Mt. Luoji; LG, Mt. Leigong; ME, Mt. Maoer; NL, Mt. Nanling; QF, Mt. Qingfengxia; QL, Mt. Qinling; SHB, Mt. Saihanba; SN, Mt. Shennongjia; SWDS, Mt. Shiwandashan; SYK, Mt. Suyukou; TM, Mt. Tianmu; WGS, Mt. Wugong; WYZ, Mt. Wuyuezhai; WZS, Mt. Wuzhi; XX, Mt. Xiaoxinganling; BD, bulk density; CIA, chemical index of alteration.

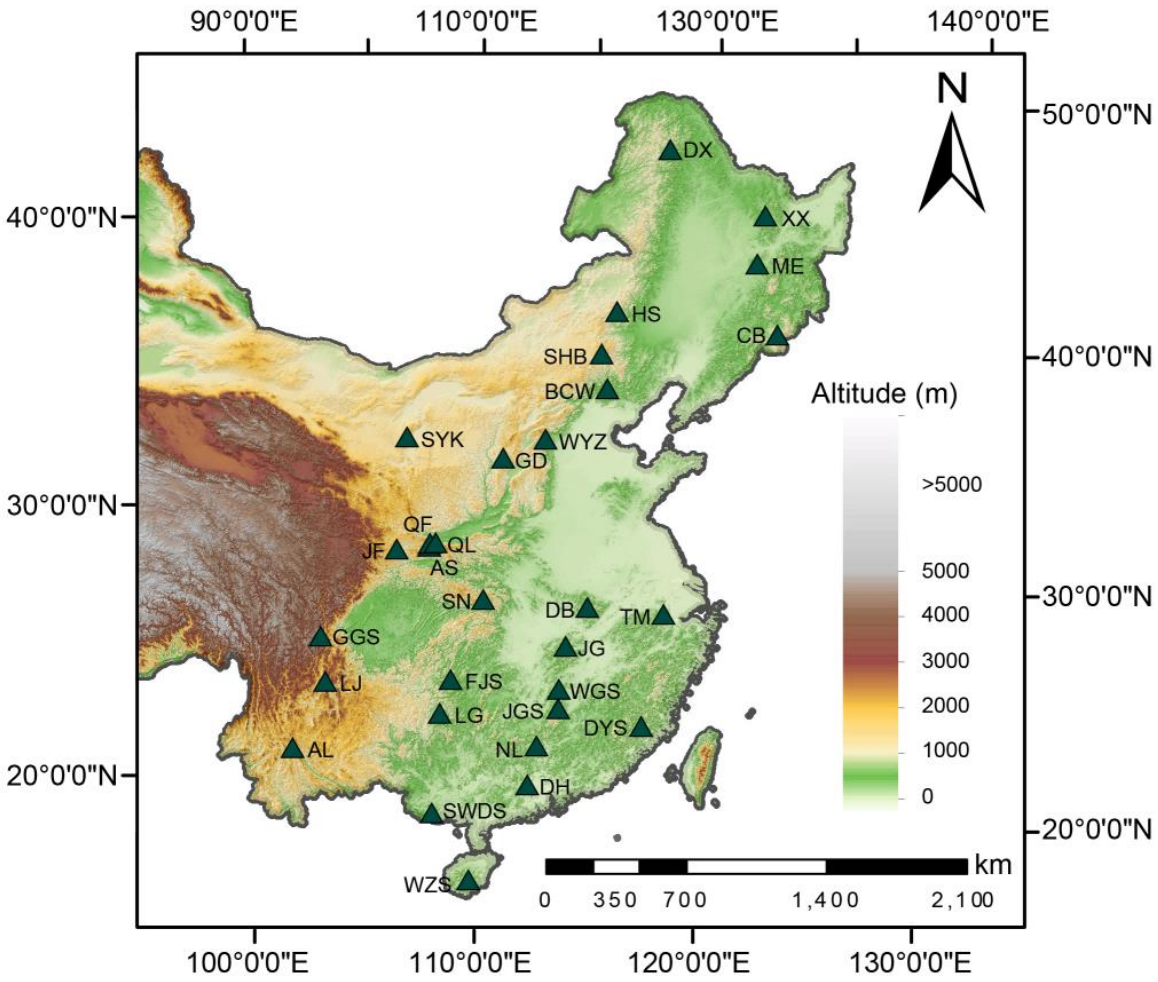

Fig. 1 Geographic distribution of the 30 China's mountains. AL, Mt. Ailao; AS, Mt. Ao; BCW, Mt. Baicaowa; CB, Mt. Changbai; DB, Mt. Dabie; DH, Mt. Dinghu; DX, Mt. Daxinganling; DYS, Mt. Daiyun; FJS, Mt. Fanjing; GD, Mt. Guandi; GGS, Mt. Gongga; HS, Mt. Han; JF, Mt. Jifeng; JG, Mt. Jiugong; JGS, Mt. Jinggang; LJ, Mt. Luoji; LG, Mt. Leigong; ME, Mt. Maoer; NL, Mt. Nanling; QF, Mt. Qingfengxia; QL, Mt. Qinling; SHB, Mt. Saihanba; SN, Mt. Shennongjia; SWDS, Mt. Shiwandashan; SYK, Mt. Suyukou; TM, Mt. Tianmu; WGS, Mt. Wugong; WYZ, Mt. Wuyuezhai; WZS, Mt. Wuzhi; XX, Mt. Xiaoxinganling.

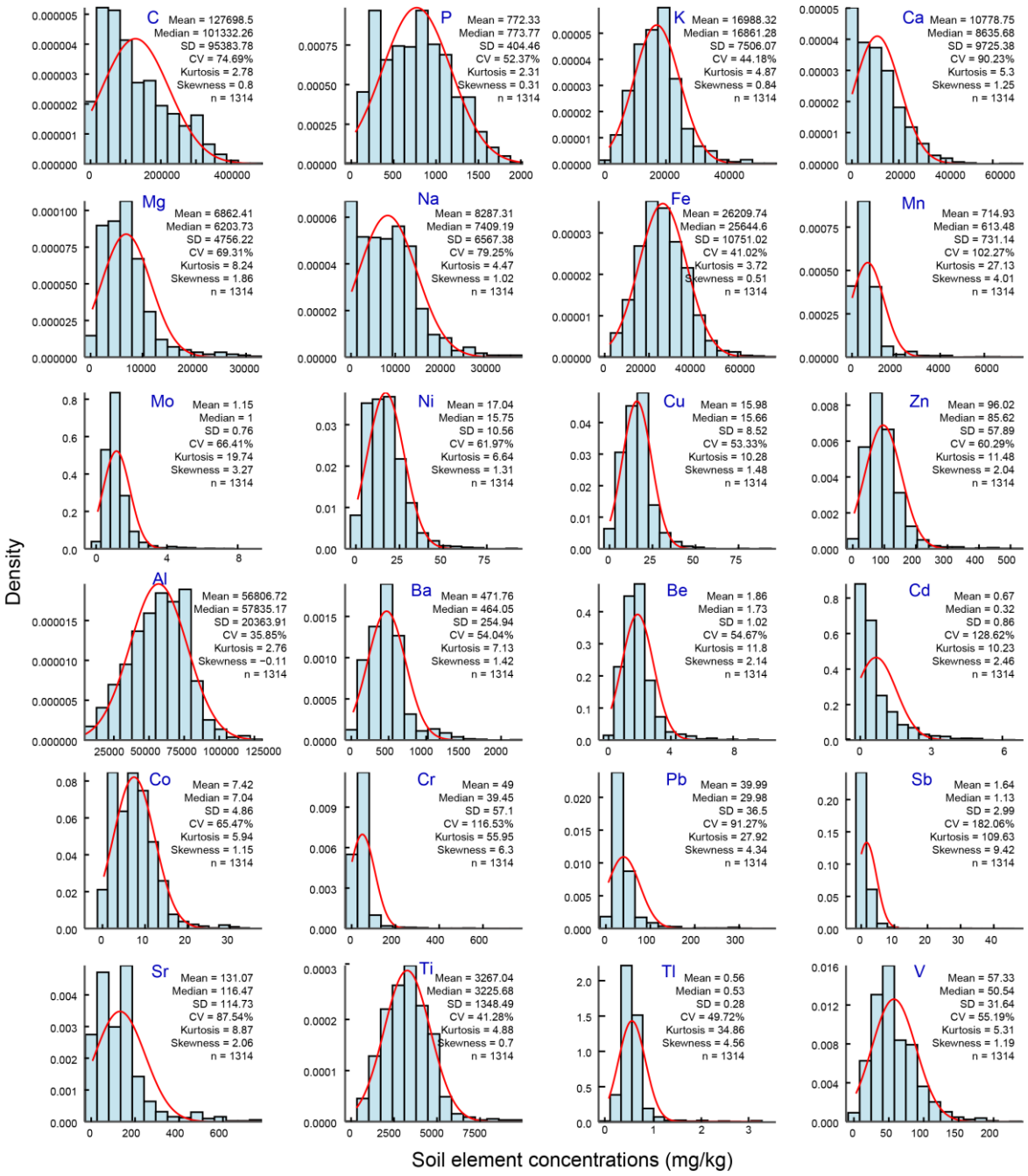

Fig. 2 Frequency distribution of soil elements across the China's mountains. Red curve on each histogram represents the fitted normal distribution. The statistical parameters of the corresponding element are annotated in the upper left of each sub-figure.

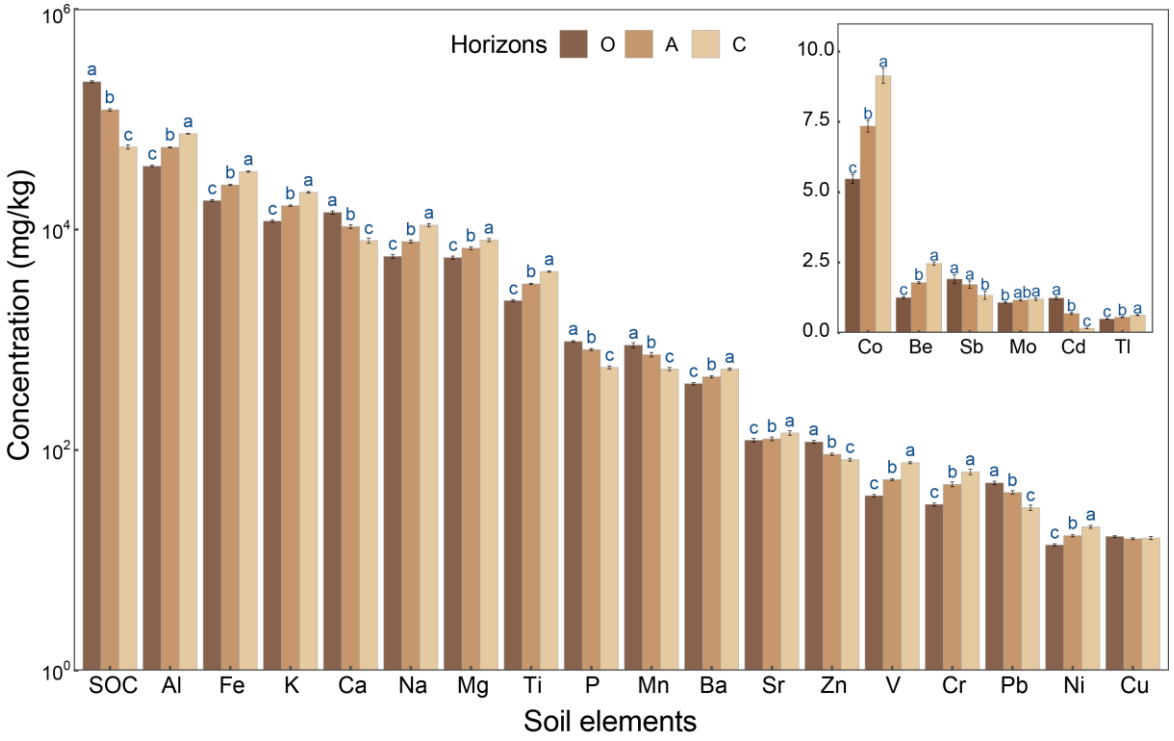

678

679 **Fig. 3** Mean concentrations of 24 elements across different soil horizons. Lowercase letters indicate

680 significant differences in each element among soil horizons ($p < 0.05$), and error bars represent the

681 standard error.

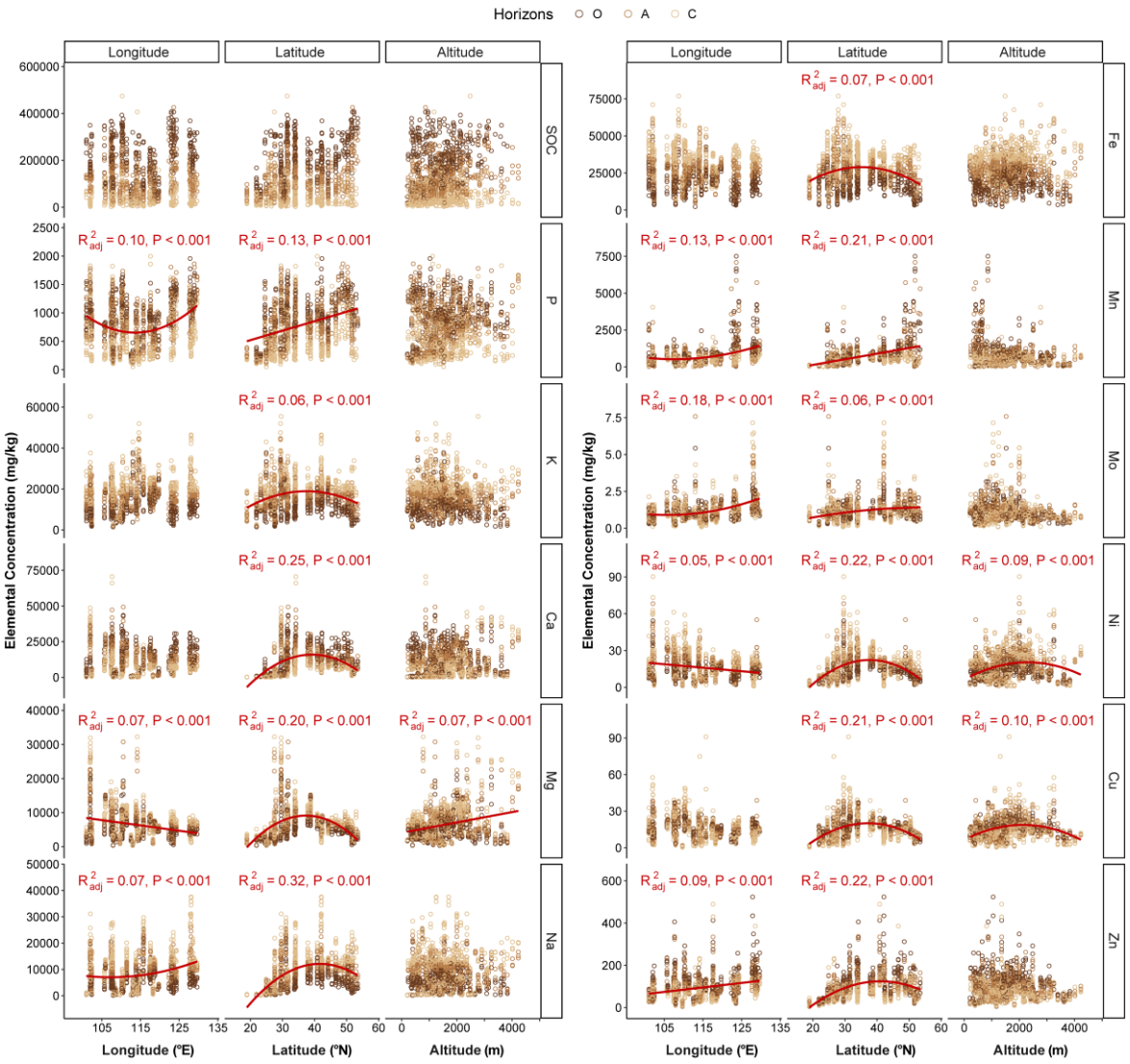
Horizons O A C
Longitude
Latitude
Altitude
SOC
P
K
Ca
Mg
Na
Fe
Mn
Mo
Ni
Cu
Zn
Elemental Concentration (mg/kg)
Longitude (°E)
Latitude (°N)
Altitude (m)

682

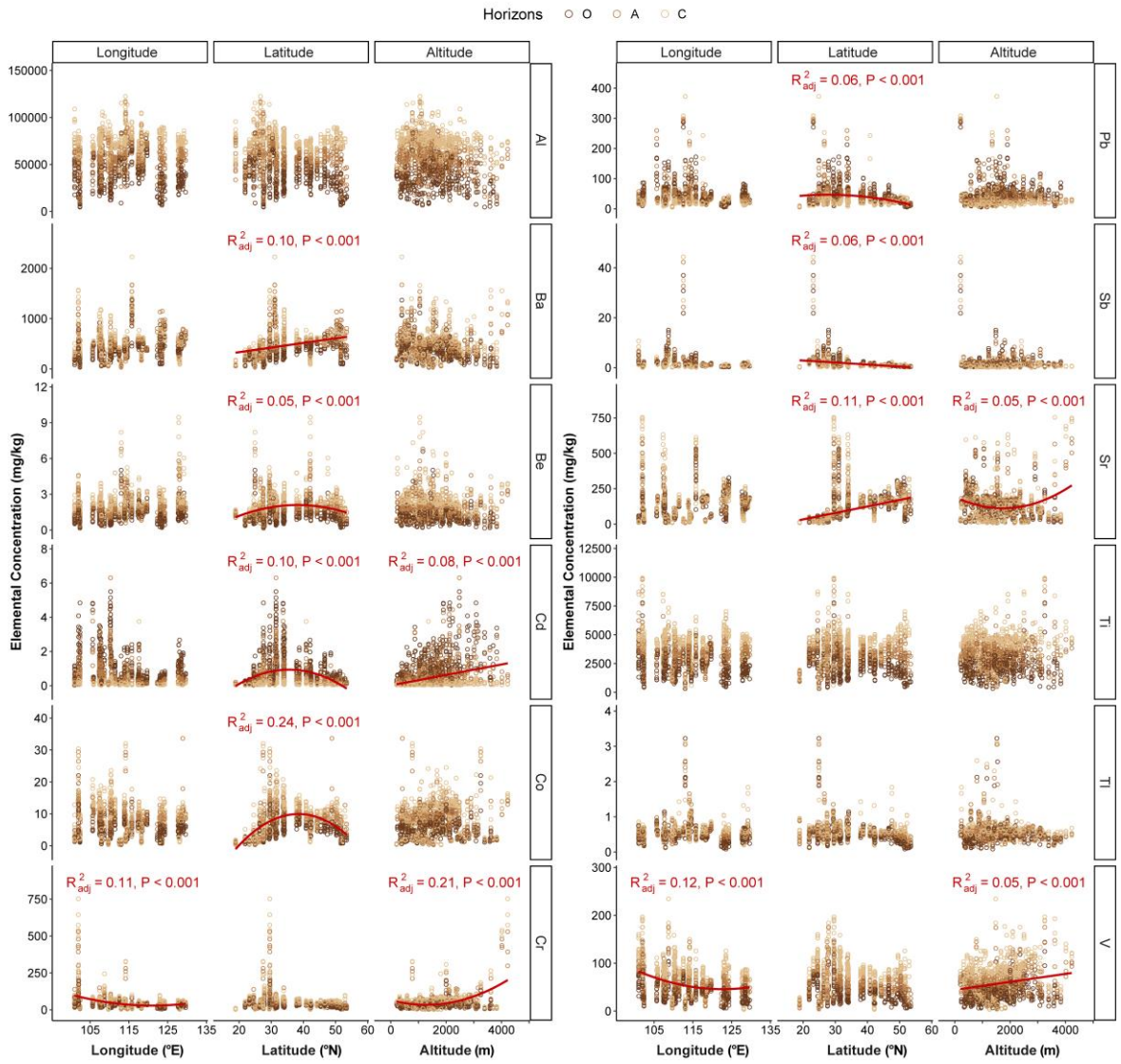

Fig. 4 Spatial distribution of soil element concentrations across latitude, longitude, and altitude. The colors of the dots represent different soil horizons. Solid red lines represent the fitting relationships of elemental concentrations with latitude, longitude, and altitude ($p<0.05$). R^2 less than 0.05 are not shown.

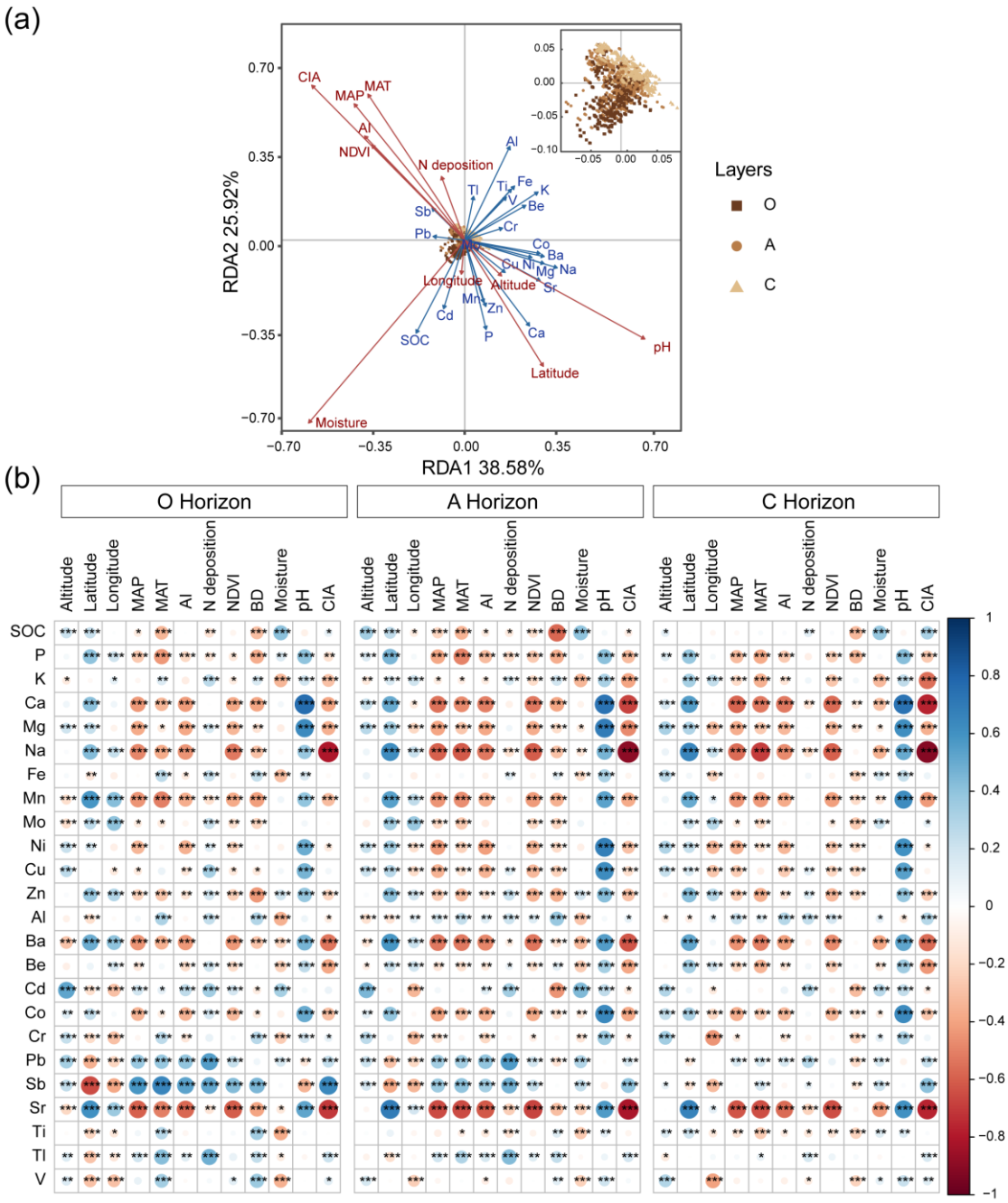

Fig. 5 The environmental factors influencing the elemental concentrations in the soils. (a) Redundancy analysis (RDA) shows the relationships of soil elements with environmental factors across soil horizons. The inserted figure shows the distribution of samples along the axes. (b) Correlation heatmap shows the correlation between soil element concentrations and environmental variables in each soil horizon. The color and circle size represent the correlation coefficient, and * indicates statistical significance ($p < 0.05$). SOC, soil organic carbon; MAP, mean annual precipitation; MAT, mean annual temperature; AI, aridity index; NDVI, normalized difference vegetation index; BD, bulk density; CIA, chemical index of alteration.

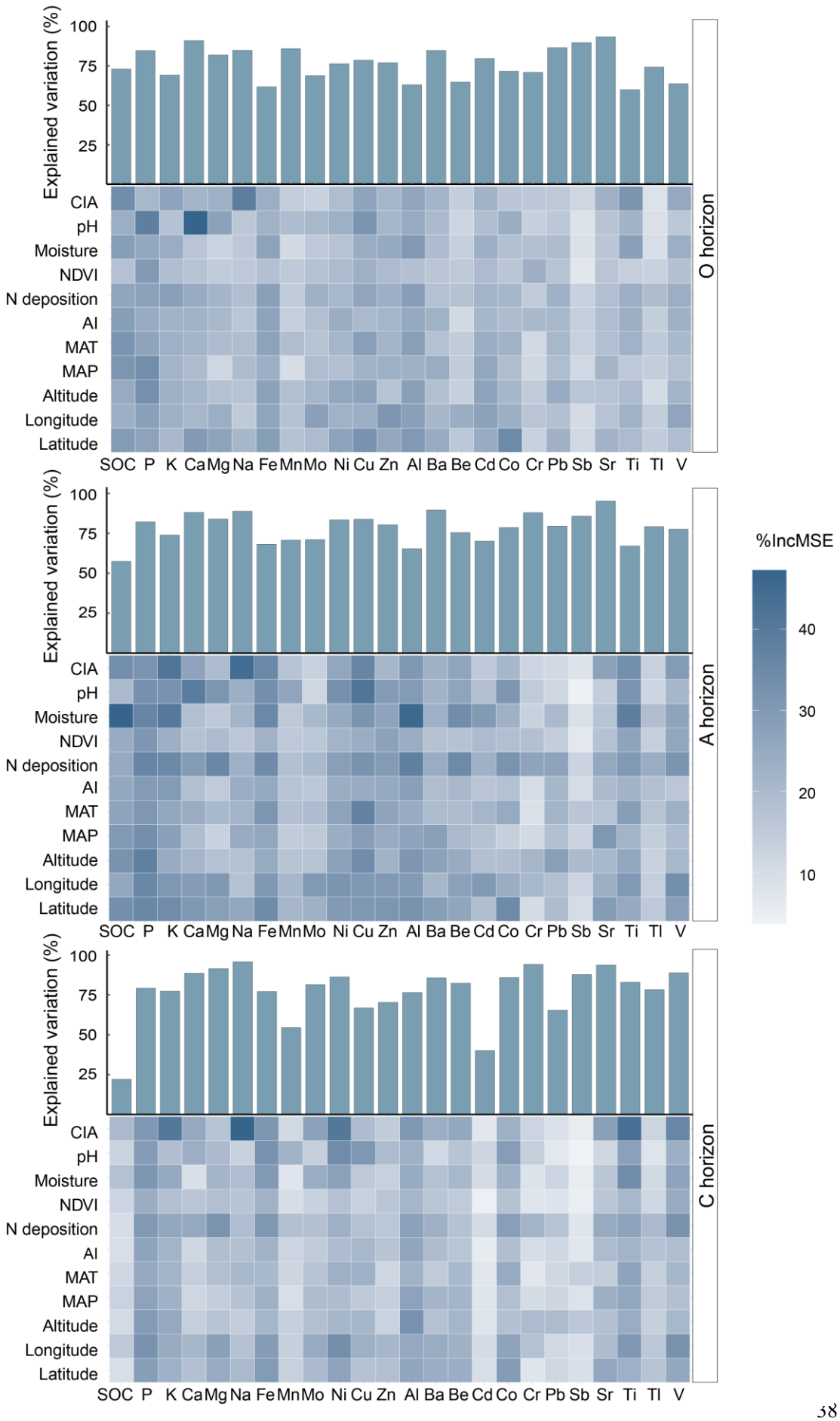
Explained variation (%)
100
75
50
25
CIA
pH
Moisture
NDVI
N deposition
AI
MAT
MAP
Altitude
Longitude
Latitude
SOC P K Ca Mg Na Fe Mn Mo Ni Cu Zn Al Ba Be Cd Co Cr Pb Sb Sr Ti Tl V
O horizon
A horizon
C horizon
%IncMSE
40
30
20
10

Fig. 6 Effects of environmental factors on elemental variability based on random forest models. The bar plots show the proportion of variance explained for individual elements. The heat maps depict the relative importance of environmental factors in predicting elemental variability, with darker shades indicating greater importance. MAP, mean annual precipitation; MAT, mean annual temperature; AI, aridity index; NDVI, normalized difference vegetation index; CIA, chemical index of alteration.